Inorganic Chemistry

Article

pubs.acs.org/IC

Experimental and Theoretical Charge Densities of a Zinc-Containing Coordination Polymer, $Zn(HCOO)_2(H_2O)_2$

Mads R. V. Jørgensen,[†] Simone Cenedese,[‡] Henrik F. Clausen,[†] Jacob Overgaard,*[,†] Yu-Sheng Chen,[§] Carlo Gatti,[‡] and Bo B. Iversen*[,†]

[†]Center for Materials Crystallography, Department of Chemistry and iNANO, Aarhus University, Langelandsgade 140, DK-8000 Aarhus C, Denmark

[‡]CNR-ISTM, Via Camillo Golgi 19, Milan, Italy

[§]ChemMatCARS, Advanced Photon Source, Argonne National Laboratory, Chicago, Illinois 60439, United States

Supporting Information

ABSTRACT: We present a combined experimental and theoretical charge density study of the coordination polymer $Zn(HCOO)_2(H_2O)_2$, which serves as a nonmagnetic reference for the isostructural magnetic compounds containing 3d transition metals. The charge density has been modeled using the multipole formalism against a high-resolution single-crystal X-ray diffraction data set collected at 100 K. The theoretical model is based on periodic density functional theory calculations in the experimental geometry. To gauge the degree of systematic bias from the multipole model, the structure factors of the theoretical model were also projected into a multipole model and the two theoretical models are compared with the experimental results. All models, both experiment and theory, show that the Zn atom densities are highly spherical but show small accumulations of charge toward the negative ligands. The metal−ligand interactions are found to be primarily ionic, but there are subtle topological indications of covalent contributions to the bonds. The source function calculated at the bond critical points reveals a rather delocalized picture of the density in the bridging carboxylates, and this presumably reflects the exchange pathway in the magnetic analogues.

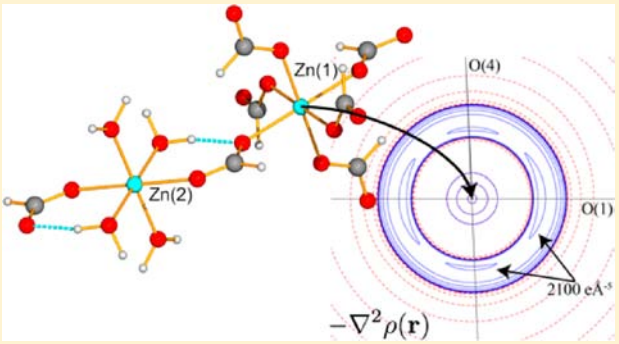

INTRODUCTION

Coordination polymers have received enormous attention because of their broad range of properties ranging from gas storage, porosity, catalytic properties, negative thermal expansion, and magnetic properties.[1] Unlike many other porous materials, the reactants are preserved during the synthesis, and thus it is, in principle, possible to tailor the product by carefully choosing the reactants. It has, however, been shown that minor changes in the synthesis parameters can lead to different products,[2] and often a given synthesis can lead to multiple products.[3] Our studies have mainly been concerned with the magnetic properties of coordination polymers through analysis of X-ray charge densities (CDs).[4] These analyses are often complicated by poor crystal quality and quite complex structures that often include disordered solvent molecules.[4c,5] This present study presents both experimental and theoretical CDs of one of the simplest coordination polymers known: $Zn(HCOO)_2(H_2O)_2$ (**1**). Isostructural compounds can be synthesized with magnesium, manganese, iron, cobalt, nickel, copper, and cadmium.[6] Part of the structure of **1** is shown in Figure 1. The compound crystallizes in the monoclinic space group $P2_1/c$ and is composed of Zn cations, formate anions, and water molecules. There are two distinct metal sites in the structure, both located on sites with inversion symmetry. Both are coordinated in a slightly distorted octahedral field by O atoms. Zn(1) is coordinated to six formate ligands, with four of these creating layers in the *bc* plane, and all Zn atoms in these layers are interconnected with formate linkers. Zn(2) is coordinated to two formate ligands and four water molecules. This creates layers of mutually unconnected Zn(2) ions interpenetrating the layers formed by Zn(1); see Figure 1b. The two kinds of layers are connected by formate linkers from Zn(1) to Zn(2), creating a three-dimensional network. The H atoms of the water molecules are all involved in hydrogen bonding; see Figure 1c. Three of these, cyan-colored, provide interaction from the Zn(1) layer to the water molecules in the Zn(2) layer. The last, shown in red in the figure, provides a contact from one Zn(2) to another Zn(2) within the same layer.

The isostructural series $M(HCOO)_2(H_2O)_2$ has been known since the 1960s,[6] and it has been studied mainly because of its interesting magnetism, which, despite a wealth of studies, is not completely understood and for which inconsistencies still exists.

Received: September 2, 2012
Published: December 10, 2012

dx.doi.org/10.1021/ic301918x | *Inorg. Chem.* 2013, 52, 297−305

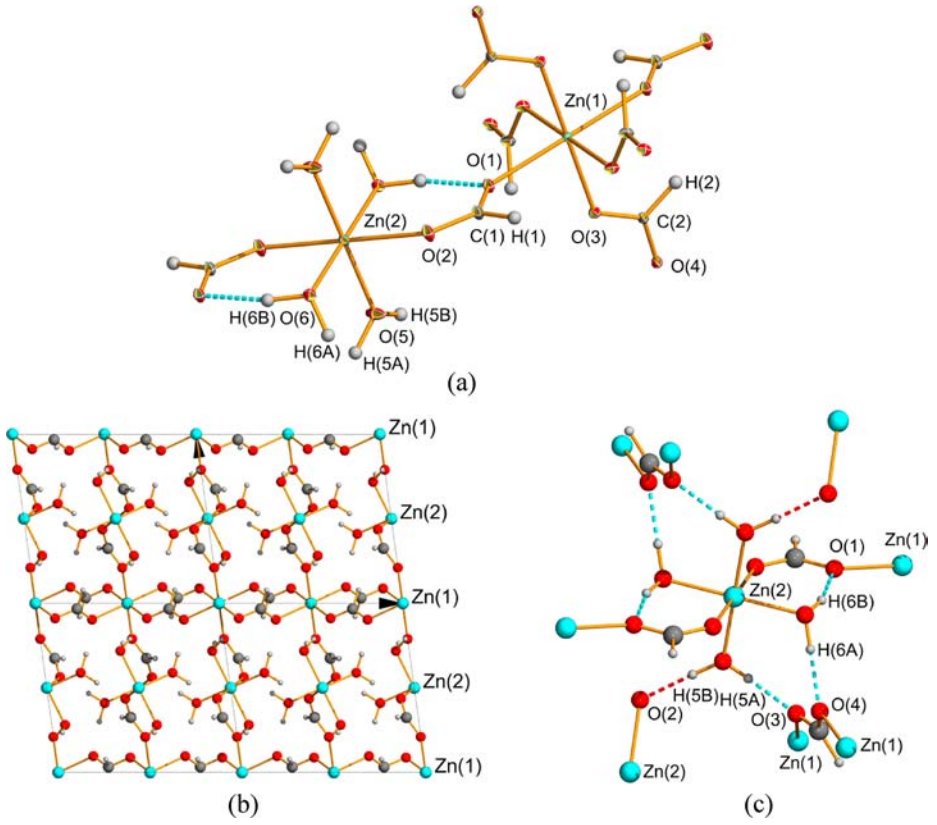

Figure 1. (a) Structure of **1** at 100 K with thermal ellipsoids at the 50% level. Labels are only shown for atoms in the asymmetric unit. (b) 2 × 2 unit cells. Projection along the *b* axis showing the alternating Zn(1) and Zn(2) layers. (c) Section of the structure showing the hydrogen bonds. The hydrogen bond within the Zn(2) layer is shown in red.

The most studied compound in the series is the manganese-containing analogue (**2**), which shows at least three phase transitions at 3.7, 1.7, and 0.6 K.[7] Because large single crystals can be grown, the microscopic magnetic structure of **2** has been studied using polarized neutron diffraction (PND).[8] Unfortunately, no estimates of the magnitude of the magnetic moments are available from the PND experiment because only reflections without antiferromagnetic contributions were measured. The various experiments revealed that the Mn(1) layers order in a canted antiferromagnetic sublattice at 3.7 K. At 1.7 K, this sublattice spontaneously reorients. The Mn(2) sublattice follows a Brillouin-like function with only slowly increasing magnetization below the Néel temperature,[7c] and it has therefore often been referred to as being paramagnetic down to 0.6 K. It has been suggested that the formate linkers act as superexchange pathways for magnetic interaction. This was supported by the PND study, where spin density was observed on the formate linkers. This suggests that covalent interactions are important for the magnetic interactions as mediators for the magnetic superexchange.[8] From heat-capacity measurements, it is found that the Mn ions correspond to high-spin Mn^{2+} ions. This agrees well with the effective magnetic moment obtained from measurements of the magnetic susceptibility, which yields 5.840(2) μ_B close to the free-ion value of 5.9 μ_B.[9] Furthermore, from analysis of the CD of $Mn(HCOO)_2(H_2O)_2$, it was concluded that both Mn ions resembles high-spin ions, supporting the magnetization measurements.[9] The nickel-containing analogue has likewise been studied by many different methods. From magnetization measurements, an effective moment of 3.14 μ_B is obtained,[10] but neutron diffraction at 1.5 K suggests much lower values of 1.7(3) and 1.3(2) μ_B for Ni(1) and Ni(2), respectively.[11] The compound in the present study is nonmagnetic and can thus be considered a reference structure, aiding the understanding of the chemical bonding and perhaps the magnetism of the compounds in the series.

In addition to being a reference to the magnetic analogues, the detailed nature of the Zn−ligand bonds is interesting in its own right because electrons in the filled 4s and 3d orbitals cannot rearrange as they would be able to in the open-shell transition-metal compounds. Various CD studies on zinc-containing compounds suggest that the nature of the Zn−X interaction can vary dramatically between compounds. Lee et al. studied crystalline $Zn(C_4O_4)(H_2O)_4$, where Zn is in an octahedral environment reminiscent of Zn(2) in **1**.[12] In this compound, Zn was found to have a charge of nearly +II along with significant deformation of the valence density. These deformations were oriented such that the negative regions, the valence-shell charge-depletion (VSCD) regions, pointed toward the ligands. The number of electrons in the d orbitals was found to be 8.4 with preferential occupancy of the t_{2g} orbitals. On the other hand, the valence-shell charge concentration (VSCC) regions around Zn oriented toward ligand Cl atoms were reported by Wang et al. However, because of the very different nature of the ligands, it is not clear whether the same bonding mechanisms apply.[13] In a recent study, Zn−O and Zn−N interactions in two Schiff base complexes showed VSCCs toward the ligands. Unfortunately, no information on the number and distribution of d electrons was given in that

dx.doi.org/10.1021/ic301918x | *Inorg. Chem.* 2013, 52, 297−305

study.[14] In other studies, highly spherical Zn ions with filled 3d orbitals have been reported.[15]

EXPERIMENTAL SECTION

Synthesis. The title compound was crystallized at the interface between a layer of formic acid (2 mL) and a solution of zinc acetate (500 mg) dissolved in water (2 mL) and ethanol (3 mL). The crystallization was performed at ambient conditions. This produces high-quality and stable colorless crystals after approximately 72 h of diffusion.

X-ray Diffraction Data Collection. A colorless crystal with dimensions of 0.125 × 0.135 × 0.195 mm^3 was mounted on a thin glass fiber using a small amount of epoxy resin. The glass fiber was glued onto a piece of copper wire attached to a brass pin. This assembly was mounted in a goniometer head and then on an Oxford Diffraction (now Agilent Technologies UK Ltd.) SuperNova system at the Department of Chemistry, Aarhus University. The sample was flash-cooled to 100(1) K using a liquid N_2 cryostream system from Oxford Cryosystems. Data were collected using ω scans with a scan width of 1°. Using the program *CrysAlisPro*,[16] a total of 111559 reflections with a resolution up to 1.15 $Å^{-1}$ were integrated and corrected for Lorentz and polarization effects. The intensities were corrected for absorption using a numerical Gaussian grid method based on the indexed faces of the sample,[17] and frame scale factors were refined using the program *ABSPACK* included in *CrysAlisPro*. Equivalent measurements were merged in *SORTAV*,[18] leading to 7227 unique reflections, corresponding to a completeness of 100%. A total of 7215 of these were measured a least three times with an overall redundancy of 15.4. Recently, it was shown that the types of microfocus X-ray tubes used in the present experiment suffer from contamination of low-energy radiation. Because the detector does not discriminate on photon energy, this contaminant radiation will add to the measured intensity.[19] This effect will yield streaks in the calculated precession images, and weak streaks are indeed visible in the images generated with this data set. The effects will be greatest for 3*h*3*k*3*l* reflections if the corresponding *hkl* reflection is intense. A comparison of the observed and calculated 3*h*3*k*3*l* reflections with intense *hkl* reflections yields no significant difference. The conclusion is the same using calculated structure factors from a *SHELXL*[20] refinement.

CD Refinement. The structure was solved using *SHELXS-97* and refined using *SHELXL-97*[20] in the program suite *WinGX*.[21] The independent atom model (IAM) from *SHELXL* was imported into *XD2006*[22] for refinement of the CD using the Hansen−Coppens multipole model (MM).[23] The initial refinement of the structural parameters, atomic coordinates, and thermal parameters was performed using only high-order reflections (sin θ/λ > 0.8 $Å^{-1}$) in order to get atomic positions less biased by nondescribed bonding density features. In subsequent refinements, the number of multipoles were gradually increased such that the final model includes all symmetry-allowed poles up to hexadecapoles for Zn atoms and octupoles for O and C atoms. All of these refinements were carried out against all data. For H atoms, a monopole and a bond-directed dipole were refined. The bond distances for H atoms were fixed to literature neutron diffraction values. κ was included in the model after inclusion of monopoles and κ' after all higher multipoles had been refined. The final model included separate κ for the two distinct Zn atoms but a common κ'. Both κ and κ' on O and C atoms are refined freely, while κ and κ' for H atoms are kept at 1.2.[24] In the end, all parameters were corefined until convergence.

To accurately model the Zn atoms, several models were tested and the residual density was scrutinized for systematic features. In previous CD studies of zinc-containing compounds, analysis was complicated because of anharmonic motion, which can correlate with the multipole parameters, thus leading to difficulties in separating vibrational and bonding features. This could lead to a masking of the detailed bonding features around the presumably highly spherical Zn atom. However, this was not the case in a recent study by Scheins et al., where it was possible to refine polarization of the 4s electrons as well as anharmonic motion.[15c] In other cases, it was indeed impossible to refine aspherical charge distribution and anharmonic motion because this leads to unphysical results.[15a,b] In the present study, there were no indications of anharmonic motion of the Zn atoms (see the Supporting Information, Figure SI1).

From overall charge considerations, the charge of each Zn atom in **1** is expected to be formally +II. Therefore, a plausible model would be to keep the $3d^{10}$ shell unperturbed and refine the population and possible aspherical features of the 4s electrons. Alternatively, the 4s electrons could be removed completely from Zn and distributed to the surrounding O atoms. This could be combined with the use of a scattering factor based on an ionic Zn. In the isostructural compound $Mn(HCOO)_2(H_2O)_2$, it was found that there was some electron donation from the ligands into the Mn 3d orbitals, thus leading to some perturbation of the atomic orbitals.[9] By analogy, the ligands could potentially perturb the valence shell and lead to an aspherical charge distribution, not only of the 4s electrons but also of the 3d electrons. Therefore, it is important to test whether the 3d electrons are indeed perturbed. Refinement with an empty 4s shell using either neutral or ionic radial functions leads to an almost spherical shell of residual density centered on both Zn atoms, indicating that the atoms have not been completely ionized and, thus, the 4s electrons must be included in the model. Residual maps of the $4s^0$ models are shown in the Supporting Information, Figure SI2. To simultaneously model both the 4s and 3d electrons, the electrons were allowed to shift between the two different orbital functions. This was realized by a valence description using the l = 0 function with a 4s radial description and the l = 2 and 4 functions with a 3d radial description. This final model yields a low $R(F^2)$ value, 1.05%, and the residual density is essentially flat and featureless. At full resolution, the maximum and minimum peaks correspond to +0.213 and −0.172 e $Å^{-3}$, respectively. Crystallographic data and refinement details are listed in Table 1. Examples of residual density maps are shown in the Supporting Information, Figure SI3.

Theoretical Calculations. The wave function was calculated using ab initio periodic density functional theory (DFT) employing the B3LYP exchange and correlation functionals[25] implemented in the

Table 1. Crystallographic Information and Refinement Details

formula	$Zn(HCOO)_2(H_2O)$
M_w (g mol^{-1})	765.82
cryst syst	monoclinic
space group	$P2_1/c$
T (K)	100
sample size (μm^3)	125 × 135 × 195
a (Å)	8.66948(3)
b (Å)	7.09008(2)
c (Å)	9.32587(4)
β (deg)	97.7185(3)
V ($Å^3$)	568.04(1)
λ(Mo Kα) (Å)	0.71073
Z	4
ρ_{calc} (g cm^{-3})	2.238
μ (mm^{-1})	4.283
T_{min}/T_{max}	0.83
unique reflns	7227 (all), 7215 ($N_{meas} \geq 3$)
sin θ/λ_{max} ($Å^{-1}$)	1.15
completeness (%)	100
$\langle N \rangle$	15.4
R_{int}	0.0276
N_{par}	269
N_{obs}	6062
$R(F)$ (%), $R(F^2)$ (%)	0.90, 1.05
$R_w(F)$ (%), $R_w(F^2)$ (%)	1.65, 3.08
GOF	0.9494

dx.doi.org/10.1021/ic301918x | *Inorg. Chem.* 2013, 52, 297−305

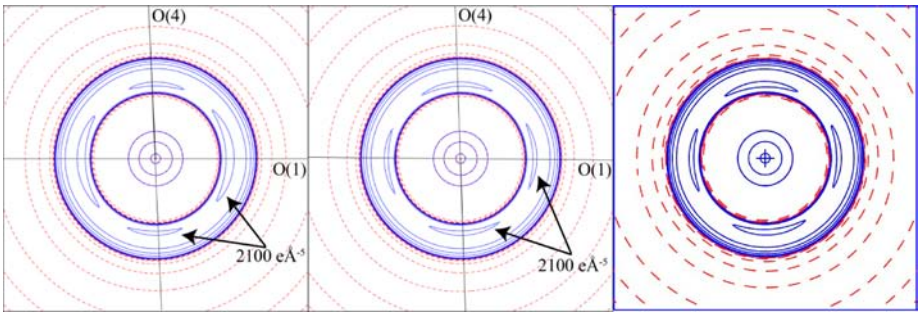

Figure 2. Laplacian profile around Zn(1). The left plot is based on the experimental data and the middle plot on the theoretical MM. The right plot is calculated directly from the wave function. The contour levels are at $\pm x \times 10^{y}$ e Å^{-5}, where x = 2, 4, 8 and y = 0, ±1, ±2. In addition to these levels, a level of ±2100 e Å^{-5} (2200 e Å^{-5} for the right plot) has been drawn. The fully drawn blue lines represent local charge accumulations, and the dashed red lines represent local charge depletion. The plots show an area of 1.1 × 1.1 Å^2.

program *CRYSTAL06*.[26] The basis set used in the calculations was a standard Pople 6-311G basis set for all atoms except Zn. The basis set for Zn was a def2-TZVP basis set,[27] overall corresponding to an all-electron triple-ζ basis. To avoid issues related to quasi-linear dependence, the coefficients of the outermost s and p functions were recalculated and the f functions were removed. The ab initio calculation was performed using the geometry obtained from the experimental CD refinement. The self-consistent-field energy convergence threshold was set to $\Delta E < 10^{-6}$ hartree. The topology of the density was analyzed using a beta version of the program *TOPOND08*.[28] To study the systematic effects of the projection of the density into the multipolar model, structure factors to a resolution matching the experiment were calculated from the theoretical density and modeled using a multipolar description equivalent to the one used to model the experimental data. This model will be referred to as the theoretical MM.

RESULTS AND DISCUSSION

Chemical Bonding. Plots of the Laplacian profile of the electron density for both the experimental and two theoretical models show nearly spherical Zn atoms with weak VSCCs; see Figure 2. These charge accumulations are also visible as positive areas in the static deformation density of the three models (not shown). For both Zn atoms in all three models, six (three unique) VSCCs are found. In all models, all points are found near the Zn−O vectors. The positions of the VSCCs are shown in Figure 3, and the density and Laplacian values at these positions are included in the Supporting Information, Table SI4.

It is interesting that the VSCCs are directed toward the negatively charged ligands and not between, as is commonly observed for other 3d transition metals.[29] During analysis of the VSCCs, it important to note that the Laplacian profile of the density around a Zn atom (like all other 3d elements) is not sufficiently sensitive to reveal the localization due to the n = 4 shell and that the last visible contraction region relates to the penultimate n = 3 shell.[30] The Laplacian profile in this region of space therefore mainly contains information about the outer core (3s and 3p) and the 3d electrons. The 3s and 3p shells are completely filled, and thus any aspherical features, VSCCs, must be due to the preferential occupation of certain 3d orbitals. The d-orbital populations can be approximated from the refined multipole populations.[31] The derivation neglects orbital hybridization and covalent effects; that is, odd-order multipoles are neglected, and the multipolar functions are assumed to be nonoverlapping. In the present crystal structure of **1**, the odd-order multipoles are forbidden by symmetry at both Zn sites.

The DFT model shows a Mulliken population of 10 electrons equally distributed in the five orbitals. The results derived from the two MMs are listed in Table 2. These both yield nearly equal populations of the different orbitals although both MMs have a slightly higher population of the e_g orbitals than the t_{2g} orbitals. This is consistent with the ligand-oriented VSCCs. Because the d orbitals are found to be virtually fully occupied (10.0(1) e), the diffuse 4s electrons must be important in the bonding interactions between Zn and the formic acid residues. This is consistent with the finding that the best MMs included the 4s electrons. The 4s population in the experimental model is refined to 2.3(2) for Zn(1) and 2.2(2) for Zn(2). The theoretical MM yield 4s populations of 1.77(5) and 1.70(5) for Zn(1) and Zn(2), respectively.

To gauge the 4s electronic population, we instead compare the Bader charges of the different models. In principle, this has

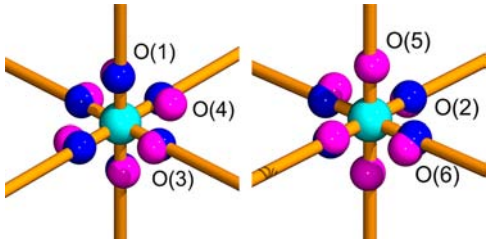

Figure 3. Position of the VSCCs around Zn(1) (left) and Zn(2) (right). Magenta spheres show positions from the experimental density and blue spheres the (overlapping) positions from both of the theoretical densities. The three VSCCs from the three models corresponding to the Zn(2)−O(5) interaction are overlapping. Bonds correspond to the interatomic vectors.

Table 2. Relative d-Orbital Population in Percent in 1[a]

	d_{z^2}	$d_{x^2-y^2}$	d_{xy}	d_{xz}	d_{yz}
$Zn(1)_{experimental}$	20.7	20.0	19.6	19.9	19.7
$Zn(1)_{MM\ theory}$	20.2	20.2	20.0	19.8	19.8
$Zn(2)_{experimental}$	20.7	20.1	19.4	19.8	20.0
$Zn(2)_{MM\ theory}$	20.1	20.3	19.9	19.9	19.8

[a]For Zn(1), the z axis is oriented toward O(1), the y axis is oriented toward O(3), and the x axis, perpendicular to z and y, is oriented close to the Zn(1)−O(4) vector. The coordinate system around Zn(2) has the z axis toward O(2), the y axis toward O(6), and the x axis close to the Zn(2)−O(5) vector. In both cases, the bond along the z axis is the longest in the octahedron and the bond near the x axis is the shortest.

dx.doi.org/10.1021/ic301918x | *Inorg. Chem.* 2013, 52, 297−305

the advantage of being model-independent because the charge is evaluated using the topology of the total density.[32] The properties of the topological atoms, defined by the zero-flux surfaces, are listed in Table 3. The Zn charge in the experimental model is quite low, 0.9 e^-, compared with that in the DFT model, which yields 1.5 e^-. The theoretical MM yields charges around 1.3 e^-; thus, part of the discrepancy between the experimental and theoretical values could be due to the projection into the MM. The 4s electrons of transition metals are notoriously hard to model because of their diffuse nature,[33] and thus often only a few low-order reflections will contain information about these electrons. These low-order reflections are often weakened by extinction, which for compound **1** has been refined to a significant value. It seems that the experimental model does include a higher population of the 4s orbital than the theoretical models. All of the charges for Zn given in Table 3 are significantly smaller than the formal II+ values, as expected for Zn with a partly populated 4s orbital.

The charges of the O atoms based on the experimental MM and DFT models show quite similar values, and overall there is a good agreement. Surprisingly, the agreement between the experimental and theoretical MMs is worse than that between the experimental and DFT models. This seems to suggest fortunate cancelation of errors in the experimental data/model. For the two C atoms, there also seems to be a large discrepancy between the three models; especially, the experimental model yields a value significantly higher than the two other models. Summing the charges for the two formate linkers and the two water molecules leads to charges of around −0.6 for the formate linkers and close to neutral charges for the water molecules.

A significant difference between the electrostatic moments obtained from the MMs and theoretical densities is found. The values are listed in the Supporting Information, Table SI5. Similar discrepancies of the moments calculated from the DFT models and MM densities were also found for $Mn(HCOO)_2(H_2O)_2$ and $Fe(HCOO)_2(H_2O)_2$.[34] The origin of this difference is not clear.

Table 3. Atomic Charges and Atomic Volumes[a]

atom	P_Ω	V_{tot}	atom	P_Ω	V_{tot}
Zn(1)	0.90	72.2	C(1)	1.68	43.9
	1.46	60.0		1.25	52.1
	1.27	64.6		1.06	54.7
Zn(2)	0.94	74.0	C(2)	1.71	44.4
	1.48	59.8		1.27	52.6
	1.26	65.4		1.07	55.2
O(1)	−1.16	102.3	H(1)	0.02	43.0
	−1.07	104.0		0.13	38.5
	−0.90	98.1		0.13	40.6
O(2)	−1.07	104.4	H(2)	0.03	41.4
	−1.05	106.6		0.11	38.4
	−0.89	101.5		0.11	39.5
O(3)	−1.16	98.9	H(5A)	0.66	10.0
	−1.06	98.5		0.55	15.2
	−0.90	94.2		0.50	17.4
O(4)	−1.11	101.9	H(5B)	0.63	10.8
	−1.06	102.2		0.57	14.7
	−0.91	98.2		0.52	16.3
O(5)	−1.26	129.9	H(6A)	0.61	12.1
	−1.11	120.7		0.55	15.6
	−1.03	120.2		0.50	17.7
O(6)	−1.16	126.8	H(6B)	0.57	14.2
	−1.09	123.4		0.54	15.8
	−0.99	120.1		0.49	18.4

[a]All entries are in atomic units. First line: experimental. Second line: theoretical. Third line: theoretical MM.

Table 4. bcp's in the Static Electron Densities[a]

bond	$\rho_b(r)$	$\nabla^2\rho(r)$	d_{1-2}	$d_{1\text{-bcp}}$	λ_1	λ_2	λ_3	ε	G	V	H	G/ρ
Zn(1)−O(1)	0.42	6.0	2.136	1.054	−1.9	−1.8	9.6	0.05	0.47	−0.52	−0.05	1.11
	0.37	6.7	2.135	1.036	−1.7	−1.6	10.0	0.03	0.46	−0.46	0.00	1.26
	0.35	6.3	2.135	1.046	−1.6	−1.6	9.4	0.03	0.43	−0.42	0.01	1.24
Zn(1)−O(3)	0.46	6.8	2.096	1.031	−2.2	−2.0	11.0	0.06	0.54	−0.61	−0.07	1.16
	0.40	7.6	2.096	1.019	−1.9	−1.9	11.4	0.03	0.53	−0.53	0.00	1.32
	0.38	7.1	2.096	1.028	−1.8	−1.8	10.7	0.03	0.49	−0.49	0.00	1.29
Zn(1)−O(4)	0.49	7.4	2.064	1.015	−2.3	−2.2	11.9	0.06	0.59	−0.67	−0.08	1.20
	0.44	8.4	2.064	1.003	−2.1	−2.1	12.6	0.04	0.59	−0.60	−0.01	1.36
	0.42	7.9	2.064	1.013	−2.1	−2.0	12.0	0.03	0.56	−0.56	0.00	1.34
Zn(2)−O(2)	0.39	5.5	2.166	1.070	−1.7	−1.6	8.8	0.04	0.43	−0.47	−0.04	1.09
	0.34	6.1	2.165	1.052	−1.5	−1.5	9.1	0.02	0.42	−0.40	0.01	1.24
	0.32	5.7	2.165	1.060	−1.4	−1.4	8.5	0.03	0.39	−0.38	0.01	1.20
Zn(2)−O(5)	0.52	7.6	2.053	1.010	−2.7	−2.4	12.6	0.12	0.62	−0.72	−0.09	1.20
	0.44	8.8	2.053	0.998	−2.2	−2.0	13.0	0.07	0.61	−0.61	0.00	1.40
	0.42	8.1	2.053	1.010	−2.2	−2.0	12.3	0.07	0.57	−0.58	0.00	1.35
Zn(2)−O(6)	0.45	6.6	2.099	1.037	−2.0	−1.9	10.5	0.06	0.52	−0.58	−0.06	1.15
	0.41	7.7	2.098	1.016	−2.0	−1.9	11.5	0.06	0.54	−0.54	0.00	1.32
	0.38	7.2	2.098	1.027	−1.8	−1.8	10.8	0.03	0.50	−0.49	0.00	1.29

[a]ρ_b (e Å^{-3}) is the electron density, $\nabla^2\rho_b$ (e Å^{-5}) the Laplacian, d_{1-2} (Å) the sum of the distances between the bcp and atomic attractors, d_{1-bcp} (Å) the distance from the first atom to the bcp, and λ_i the eigenvalues of the Hessian matrix at the bcp. ε is the ellipticity. G, V, and H are the kinetic energy density, the potential energy density, and the total energy density (hartree Å^{-3}) derived using the Abramov functional.[38] The random errors estimated from the least-squares procedure are typically on the third decimal for ρ and $\nabla^2\rho$. This is much smaller (by an order of magnitude) than the systematic error because of the specific choice of the density model. Therefore, we only list the values to the second decimal in ρ and the first decimal in $\nabla^2\rho$. The first line contains the experimental results, the second line the theoretical results, and the third line the results from the theoretical MMs.

dx.doi.org/10.1021/ic301918x | Inorg. Chem. 2013, 52, 297−305

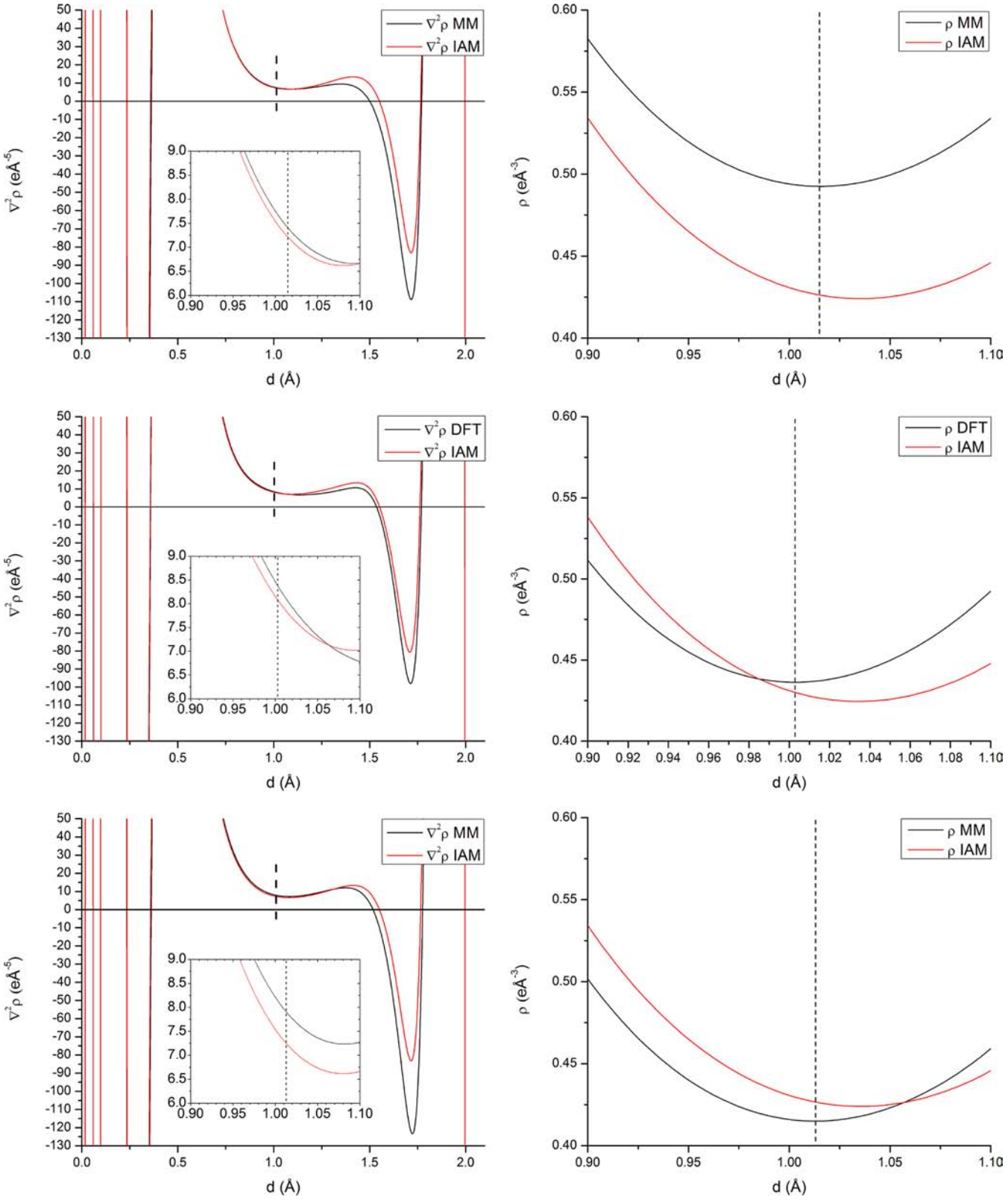

Figure 4. Plots of the Laplacian (left column) and electron density (right column) profiles along the Zn(1)−O(4) interaction. The inset in the Laplacian profile show an enlarged view near the bcp. The first row corresponds to the experimental MM, the second row to the DFT model, and the third row to the theoretical MM. Black lines show the MM/DFT results, and red lines show the IAM results. Dashed vertical lines show the position of the bcp in the MM/DFT densities.

The properties at the bond critical points (bcp's) of the Zn−O interactions are listed in Table 4. The Zn−O bonds all have a low density at the bcp and a positive value of $\nabla^2\rho$. The experimental densities show a slightly negative value of the total energy density, H, whereas the theoretical densities show a value very close to 0. The best agreement is found between the

dx.doi.org/10.1021/ic301918x | *Inorg. Chem.* 2013, 52, 297−305

two theoretical models, and it does not seem that all of the discrepancies between the experimental and DFT results are due to projection into the multipole functions. The major part of the difference in Laplacian value is due to a lower value of λ_3 in the experiments, meaning a smaller depletion of the density along the bond compared with the theoretical density. The values of the density at the bcp's are increasing with decreasing bond lengths. This is accompanied by an increase of the Laplacian value due to a density increase in the charge-depletion region.[35]

Classification of the bonds using the sign of the Laplacian[36] profile would argue for closed-shell ionic interactions. Using the ratio between the kinetic and potential energy densities, $|V_b|/G_b$, classifies the bonds in the "transit region", indicating bonds that show a resemblance of closed-shell ionic bonds, with some degree of "incipient covalence".[37] This incipient covalency was also observed for the isostructural manganese-containing system, although the Mn−O bonds showed a positive energy density at the bcp.[9] This could indicate that the Zn−O bonds are more covalent than the Mn−O bonds. The metal−O distances in **1** are shorter than those in the manganese compound, which should ensure a larger overlap of orbitals, thus potentially leading to a more covalent interaction. Some degree of covalency is expected because the magnetic ordering of the isostructural systems is mediated by superexchange through the formate linkers.[8] All Zn−O bonds are quite similar, but a small difference is observed between the Zn(2)−O(5) and Zn(2)−O(6) bonds. This is mainly due to the geometry of the water molecules, where the Zn−O vector is located between the two expected lone pairs on O(5) and toward a lone pair on O(6). This is most easily seen in the ellipticity, which is larger for Zn(2)−O(5) than Zn(2)−O(6), revealing a less cylindrical charge distribution at the bcp for the former.

Because the bcp is located in the valence-shell depletion region of both the Zn and O atoms, the absolute value of the Laplacian profile in the Zn−O bond is not a good descriptor for the degree of covalency in the bonds, caused by the 4s electrons, because the outermost valence shell is not visible in the Laplacian.[30,39] Therefore, it is informative to compare the Laplacian profile in **1** to that of a nonbonded reference, e.g., an IAM model. The density and Laplacian profiles along the Zn(1)−O(4) bond for the three models and the IAM model are shown in Figure 4.

From the Laplacian profiles, it can be seen that the MM/DFT densities show a larger value of the Laplacian at the bcp compared with the IAM model, corresponding to a higher depletion at the bcp. This is observed as a lower value of λ_3 in the IAM mode compared to the MM/DFT densities. It can also be seen that the VSCC for O (around 1.7 Å) is more pronounced in the MM model, and the VSCD region (at 1.4 Å) is slightly less depleted. This is expected due to charge transfer from Zn to O. Charge transfer from Zn to the O atoms is also visible in the ρ profiles, where there is a shift of the profile toward the Zn atom in the MM/DFT densities compared to the IAM density. The shift in the experimental MM is not as large as that in the two other models, leading to a large Zn−bcp distance and a corresponding larger volume of the atomic basin; see Table 3. The value of the density at the bcp (in the MM/DFT density) is higher than the IAM value for the experimental model, slightly higher for the DFT model, and slightly lower for the theoretical MM. It is quite curious that the density from the theoretical MM is lower than the IAM density; one reason could be the slight difference in the refined expansion/contraction parameters in the MMs. For both models, both the core and valence shell is contracted, $\kappa^{(\prime)} < 1$; see Table 5.

Table 5. Refined Expansion/Contraction Parameters for the Zn Atoms in the Two MMs

	experimental MM		theoretical MM	
	κ	κ'	κ	κ'
Zn(1)	0.977(4)	0.95(4)	0.997(1)	0.84(1)
Zn(2)	0.970(4)	0.95(4)	0.997(1)	0.85(1)

The spherical valence is most contracted in the experimental model, whereas the aspherical valence is more contracted in the theoretical MM. Substituting the experimental values into the theoretical model leads to a slight increase of the density at the bcp, but the value is still smaller than the IAM value.

Zn(1)−O(4) is the shortest bond in the Zn(1) coordination sphere. The Laplacian and density profiles for the longer Zn(1)−O(1) bond is included in the Supporting Information, Figure SI7. These profiles show the same behavior as that seen for Zn(1)−O(4).

Considering the negative or near-zero value of the total energy density, the nonzero 4s population, the ligand-directed VSCCs, and the increase in ρ and $\nabla^2\rho$ at the bcp's compared with the IAM density (for the experimental and DFT models), it seems clear that the Zn−O interactions include both electrostatic and covalent effects. The main contributor must be electrostatic, but several indicators show that the interactions are not entirely so. The weak ligand-directed VSCCs are presumably only visible because of the nearly spherical charge distribution of Zn. An open d-shell transition metal would lead to much more dominant features in the valence shell, thus hiding the finer features seen here, as is also seen, for instance, in the manganese-containing analogue.[9]

It is anticipated that any superexchange interaction between the metal centers through the formate linkers would require electronic communication in the form of delocalization. To study this effect, we have calculated the source function (SF)[37c,40] contributions for the different atoms at the various bcp's in the formate linker from Zn(1) to Zn(1) or Zn(2). The experimental and theoretical values show overall good agreement (Table 6 and Figure 5). It is found that the Zn atoms only contribute significantly to the adjacent Zn−O bcp's with approximately 30% of the density. The O atom adjacent to the bcp also contributes with approximately 30% of the density. Very interestingly, it is found that both the C atom and the opposed O atom contribute significantly to the bcp. This is found for both of the Zn−OCO−Zn pathways, i.e., intra- and interlayer directions. In essence, this shows that the formate linker is capable of "exchanging information" from one Zn atom to the next. Because the present study concerns a nonmagnetic compound, it will be interesting to study the SF in the isostructural, but magnetic analogues. This is the subject of an ongoing study.

CONCLUSIONS

The CD of the coordination polymer **1** was modeled against a high-resolution X-ray diffraction data set collected at a conventional source at 100 K. Using the experimental geometry, a theoretical electron density distribution was obtained using fully periodic DFT calculations. In general, there is a good agreement between the experimental and theoretical densities. In the literature, the electron density of Zn

dx.doi.org/10.1021/ic301918x | Inorg. Chem. 2013, 52, 297−305

Table 6. Theoretical SF Contributions in Percent from Various Atoms of the Density at the Different bcp Positions in Figure 5[a]

bcp	Zn(1)	Zn(2)	O(1)	O(2)	O(6)	C(1)	H(1)	H(5)	H(6)
B3	**27.53**	−0.14	**30.91**	**6.42**	−0.20	**5.02**	2.74	0.14	−2.18
B7	−0.01	−0.04	**47.97**	**7.27**	−0.07	**39.69**	2.91	0.04	−0.34
B9	−0.06	−0.04	**6.00**	**6.37**	−0.11	**42.64**	**42.78**	0.03	−0.20
B8	−0.03	−0.03	**6.91**	**48.43**	−0.11	**40.03**	2.90	0.05	−0.19
B6	−0.13	**25.56**	4.63	**28.30**	0.33	**7.42**	3.52	1.51	0.95
B18	−0.15	−0.27	**26.16**	**5.29**	**37.88**	**9.54**	4.92	4.11	−2.25
B16	−0.02	0.06	−0.16	0.09	**56.13**	0.59	0.43	1.55	**38.80**
B5	−0.10	**29.80**	0.12	−0.73	**35.06**	2.37	1.81	**5.03**	**5.42**
B15	−0.02	0.05	−0.24	−0.05	**56.62**	0.29	0.26	**39.23**	1.55

bcp	Zn(1)	O(3)	O(4)	C(2)	H(2)	Zn(1)
B1	**31.12**	**5.76**	**32.86**	4.67	2.41	−0.07
B11	0.09	**7.21**	**48.07**	**39.40**	2.92	−0.01
B12	0.00	**6.19**	**6.17**	**42.39**	**42.66**	−0.04
B10	0.02	**48.36**	**6.96**	**39.39**	2.83	0.03
B2	−0.04	**31.36**	**5.89**	**5.01**	2.60	**29.53**

[a]All contributions above 5% are marked in bold. The theoretical values are in good agreement with the experimental values. The absolute values of the SF contribution at the adjacent Zn−O bcp were found to be quite dependent on the radius of the β sphere. The values shown here were obtained with a small β sphere (r = 0.5 Å) to increase the precision.

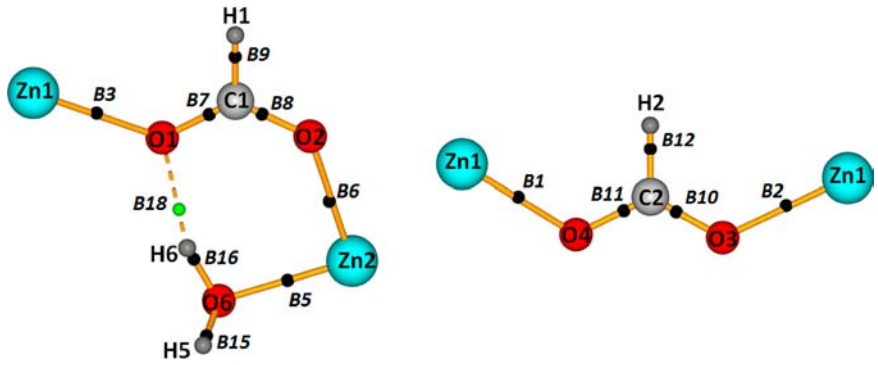

Figure 5. Nomenclature of the bcp used in SF calculations.

atoms in various compounds varies greatly from highly spherical to distorted ions. In **1**, the Zn atoms are quite spherical, with subtle aspherical features. The density of Zn atoms shows valence-shell charge accumulations toward the O atoms of the ligands. Overall, the density of Zn atoms in **1** shows weak valence-shell charge accumulations toward the O atoms of the ligands. This is corroborated by the populations of the d orbitals, which are slightly higher for the ligand-directed e_g orbitals than the t_{2g} orbitals. All models show that the 4s electrons are important for bonding of the ligands to the Zn atoms. Analysis of the Laplacian and density profiles indicates covalent features in the primarily ionic metal−ligand interactions. Analysis of the SF contributions at the bcp's corroborates a quite delocalized bonding pattern across the formate bridges and directly shows the presumed covalent exchange pathway in magnetic analogues.

■ ASSOCIATED CONTENT

Supporting Information

Anharmonic motion of O(5) in **1**, residual density maps of **1**, residual density maps from MMs of **1** having $4s^0$ configurations with neutral (Zn^0) and ionic (Zn^{2+}) radial functions, VSCC of zinc, dipole and quadrupole moments of the atomic basins, bcp properties, and Laplacian and electron density profiles along Zn(1)−O(1). This material is available free of charge via the Internet at http://pubs.acs.org.

■ AUTHOR INFORMATION

Corresponding Author

*E-mail: bo@chem.au.dk (B.B.I.), jacobo@chem.au.dk (J.O.).

Notes

The authors declare no competing financial interest.

■ ACKNOWLEDGMENTS

This work was supported by the Danish National Research Foundation (Center for Materials Crystallography) and the Danish Strategic Research Council (Center for Energy Materials).

■ REFERENCES

(1) (a) Weng, D.-F.; Wang, Z.-M.; Gao, S. *Chem. Soc. Rev.* **2011**, *40*, 3157−3181. (b) Sculley, J.; Yuan, D.; Zhou, H.-C. *Energy Environ. Sci.* **2011**, *4*, 2721−2735. (c) Ranocchiari, M.; van Bokhoven, J. A. *Phys. Chem. Chem. Phys.* **2011**, *13*, 6388−6396. (d) Meek, S. T.; Greathouse, J. A.; Allendorf, M. D. *Adv. Mater. (Weinheim, Germany)* **2011**, *23*, 249−267. (e) Martinez, C.; Corma, A. *Coord. Chem. Rev.* **2011**, *255*, 1558−1580. (f) Dechambenoit, P.; Long, J. R. *Chem. Soc. Rev.* **2011**, *40*, 3249−3265. (g) Coudert, F.-X.; Boutin, A.; Jeffroy, M.; Mellot-Draznieks, C.; Fuchs, A. H. *ChemPhysChem* **2011**, *12*, 247−258. (h) Zhou, W. *Chem. Rec.* **2010**, *10*, 200−204. (i) Ma, S.; Zhou, H.-C. *Chem. Commun. (Cambridge, U. K.)* **2010**, *46*, 44−53. (j) Lock, N.; Wu, Y.; Christensen, M.; Cameron, L. J.; Peterson, V. K.; Bridgeman, A. J.; Kepert, C. J.; Iversen, B. B. *J. Phys. Chem. C* **2010**, *114*, 16181−

16186. (k) Peterson, V. K.; Kearley, G. J.; Wu, Y.; Ramirez-Cuesta, A. J.; Kemner, E.; Kepert, C. J. *Angew. Chem., Int. Ed.* **2010**, *49*, 585−588.
(2) Edgar, M.; Mitchell, R.; Slawin, A. M. Z.; Lightfoot, P.; Wright, P. A. *Chem.—Eur. J.* **2001**, *7*, 5168−5175.
(3) Clausen, H. F.; Poulsen, R. D.; Bond, A. D.; Chevallier, M. A. S.; Iversen, B. B. *J. Solid State Chem.* **2005**, *178*, 3342−3351.
(4) (a) Poulsen, R. D.; Bentien, A.; Chevalier, M.; Iversen, B. B. *J. Am. Chem. Soc.* **2005**, *127*, 9156−9166. (b) Poulsen, R. D.; Bentien, A.; Graber, T.; Iversen, B. B. *Acta Crystallogr., Sect. A: Found. Crystallogr.* **2004**, *60*, 382−389. (c) Clausen, H. F.; Overgaard, J.; Chen, Y. S.; Lversen, B. B. *J. Am. Chem. Soc.* **2008**, *130*, 7988−7996.
(5) (a) Jørgensen, M. R. V.; Clausen, H. F.; Christensen, M.; Poulsen, R. D.; Overgaard, J.; Iversen, B. B. *Eur. J. Inorg. Chem.* **2011**, 549−555. (b) Meindl, K.; Henn, J.; Kocher, N.; Leusser, D.; Zachariasse, K. A.; Sheldrick, G. M.; Koritsanszky, T.; Stalke, D. *J. Phys. Chem. A* **2009**, *113*, 9684−9691.
(6) Osaki, K.; Nakai, Y.; Watanabe, T. *J. Phys. Soc. Jpn.* **1963**, *18*, 919.
(7) (a) Flippen, R. B.; Friedberg, S. A. *J. Chem. Phys.* **1963**, *38*, 2652−2657. (b) Abe, H.; Matsuura, M. *J. Phys. Soc. Jpn.* **1964**, *19*, 1867−1880. (c) Pierce, R. D.; Friedberg, S. A. *Phys. Rev.* **1968**, *165*, 680−686. (d) Abe, H.; Matsuura, M.; Morigaki, H.; Yamagata, K.; Torii, K. J. *Phys. Soc. Jpn.* **1964**, *19*, 775−776. (e) Abe, H.; Torii, K. *J. Phys. Soc. Jpn.* **1965**, *20*, 183−184. (f) Bertaut, E. F.; Burlet, P. *Solid State Commun.* **1969**, *7*, 343−349. (g) Yamagata, K. *J. Phys. Soc. Jpn.* **1967**, *22*, 582−589. (h) Burlet, P.; Bertaut, E. F.; Roult, G.; Decombar, A.; Pillon, J. *J. Solid State Commun.* **1969**, *7*, 1403−1408.
(8) Radhakrishna, P.; Gillon, B.; Chevrier, G. *J. Phys.: Condens. Matter* **1993**, *5*, 6447−6460.
(9) Poulsen, R. D.; Jorgensen, M. R. V.; Overgaard, J.; Larsen, F. K.; Morgenroth, W. G.; Graber, T.; Chen, Y. S.; Iversen, B. B. *Chem.—Eur. J.* **2007**, *13*, 9775−9790.
(10) Kageyama, H.; Khomskii, D. I.; Levitin, R. Z.; Vasil'ev, A. N. *Phys. Rev. B* **2003**, *67*, 224422.
(11) Jørgensen, M. R. V.; Christensen, M.; Schmøkel, M. S.; Iversen, B. B. *Inorg. Chem.* **2011**, *50*, 1441−1446.
(12) Lee, C. R.; Wang, C. C.; Chen, K. C.; Lee, G. H.; Wang, Y. J. *Phys. Chem. A* **1999**, *103*, 156−165.
(13) Wang, R. M.; Lehmann, C. W.; Englert, U. *Acta Crystallogr., Sect. B: Struct. Crystallogr. Cryst. Chem.* **2009**, *65*, 600−611.
(14) Kotova, O.; Lyssenko, K.; Rogachev, A.; Eliseeva, S.; Fedyanin, I.; Lepnev, L.; Pandey, L.; Burlov, A.; Garnovskii, A.; Vitukhnovsky, A.; Van der Auweraer, M.; Kuzmina, N. *J. Photochem. Photobiol., A* **2011**, *218*, 117−129.
(15) (a) Spasojević-de Biré, A.; Bouhmaida, N.; Kremenović, A.; Morgant, G.; Ghermani, N. E. *J. Phys. Chem. A* **2002**, *106*, 12170−12177. (b) Novaković, S. B.; Bogdanović, G. A.; Fraisse, B.; Ghermani, N. E.; Bouhmaida, N.; Spasojević-de Biré, A. *J. Phys. Chem. A* **2007**, *111*, 13492−13505. (c) Scheins, S.; Zheng, S. L.; Benedict, J. B.; Coppens, P. *Acta Crystallogr., Sect. B: Struct. Crystallogr. Cryst. Chem.* **2010**, *66*, 366−372.
(16) Agilent Technologies UK Ltd. *CrysAlisPro*, 171.34.44; Agilent Technologies UK Ltd.: Berkshire, U.K., 2010.
(17) Clark, R. C.; Reid, J. S. *Acta Crystallogr., Sect. A: Found. Crystallogr.* **1995**, *51*, 887−897.
(18) Blessing, R. H. *J. Appl. Crystallogr.* **1997**, *30*, 421−426.
(19) Macchi, P.; Burgi, H. B.; Chimpri, A. S.; Hauser, J.; Gal, Z. *J. Appl. Crystallogr.* **2011**, *44*, 763−771.
(20) Sheldrick, G. M. *Acta Crystallogr., Sect. A: Found. Crystallogr.* **2008**, *64*, 112−122.
(21) Farrugia, L. *J. Appl. Crystallogr.* **1999**, *32*, 837−838.
(22) Volkov, A.; Macchi, P.; Farrugia, L. J.; Gatti, C.; Mallinson, P.; Richter, T.; Koritsanszky, T. *XD2006*, revision 5.34; University at Buffalo, State University of New York, Buffalo, NY, University of Milano, Milano, Italy, University of Glasgow, Glasgow, U.K., CNR-ISTM, Milano, Italy, and Middle Tennessee State University, Murfreesboro, TN, 2006.
(23) Hansen, N. K.; Coppens, P. *Acta Crystallogr., Sect. A: Found. Crystallogr.* **1978**, *34*, 909−921.
(24) Stewart, R. F.; Davidson, E. R.; Simpson, W. T. *J. Chem. Phys.* **1965**, *42*, 3175−3187.
(25) (a) Becke, A. D. *J. Chem. Phys.* **1993**, *98*, 5648−5652. (b) Lee, C. T.; Yang, W. T.; Parr, R. G. *Phys. Rev. B* **1988**, *37*, 785−789.
(26) Dovesi, R.; Saunders, V. R.; Roetti, C.; Orlando, R.; Zicovich-Wilson, C. M.; Pascale, F.; Civalleri, B.; Doll, K.; Harrison, N. M.; Bush, I. J.; D'Arco, P.; Llunell, M. *CRYSTAL06 User's Manual*; University of Turin: Turin, Italy, 2006.
(27) Weigend, F.; Ahlrichs, R. *Phys. Chem. Chem. Phys.* **2005**, *7*, 3297−3305.
(28) Gatti, C. *TOPOND08, β version*; 2009; unpublished.
(29) Farrugia, L. J.; Evans, C. *C. R. Chim.* **2005**, *8*, 1566−1583.
(30) Sagar, R. P.; Ku, A. C. T.; Smith, V. H.; Simas, A. M. *J. Chem. Phys.* **1988**, *88*, 4367−4374.
(31) Holladay, A.; Leung, P.; Coppens, P. *Acta Crystallogr., Sect. A: Found. Crystallogr.* **1983**, *39*, 377−387.
(32) Bader, R. F. W. *Atoms in molecules: a quantum theory*; Oxford University Press: New York, 1990.
(33) Figgis, B. N.; Iversen, B. B.; Larsen, F. K.; Reynolds, P. A. *Acta Crystallogr., Sect. B: Struct. Crystallogr. Cryst. Chem.* **1993**, *49*, 794−806.
(34) Jørgensen, M. R. V. *Charge Density Studies of Magnetic Coordination Polymers*; Aarhus University: Aarhus, Denmark, 2011.
(35) (a) Gatti, C.; Lasi, D. *Faraday Discuss.* **2007**, *135*, 55−78. (b) Overgaard, J.; Hibbs, D. E.; Rentschler, E.; Timco, G. A.; Larsen, F. K. *Inorg. Chem.* **2003**, *42*, 7593−7601.
(36) Bader, R. F. W.; Essen, H. *J. Chem. Phys.* **1984**, *80*, 1943−1960.
(37) (a) Espinosa, E.; Alkorta, I.; Elguero, J.; Molins, E. *J. Chem. Phys.* **2002**, *117*, 5529−5542. (b) Macchi, P.; Sironi, A. *Coord. Chem. Rev.* **2003**, *238*−*239*, 383−412. (c) Gatti, C. *Z. Kristallogr.* **2005**, *220*, 399−457.
(38) Abramov, Y. A. *Acta Crystallogr., Sect. A: Found. Crystallogr.* **1997**, *53*, 264−272.
(39) Shi, Z.; Boyd, R. J. *J. Chem. Phys.* **1988**, *88*, 4375−4377.
(40) Bader, R. F. W.; Gatti, C. *Chem. Phys. Lett.* **1998**, *287*, 233−238.